# ANTIWINDUP AND OVERRIDE CONTROL FOR EXPONENTIALLY UNSTABLE SYSTEMS WITH ACTUATOR CONSTRAINTS

**Adolf Hermann Glattfelder, Walter Schaufelberger**

*Automatic Control Lab, ETH Zürich, Switzerland,*
*glatt@control.ee.ethz.ch, ws@control.ee.ethz.ch*

Abstract: Control of exponentially unstable plants with an actuator having both position and rate saturations is investigated. The standard antiwindup technique is not able to increase the very limited radius of attraction. A novel design technique based on the override technique is proposed which enlarges the radius of attraction, such that the actuator working range can be utilized. 

Keywords: Exponentially unstable systems, Input and Output Constraint Control, Nonlinear Stability Analysis, Antiwindup, Override Control.

## 1. INTRODUCTION

The closed loop performance of linear control systems may deteriorate if the actuator constraints are met. This is the case for asymptotically stable plants and even more so for exponentially unstable plants, where the area of attraction can be so small that even routine deviations may result in divergent behavior. Therefore constrained control of exponentially unstable systems has become of research interest recently, e.g. (Barbu *et al.*, 2002), (Tarbouriech and Garcia, 2002).
The graphic circle test (Khalil, 2002) is used for the analysis and design of control loops with saturating static actuators and stable plants with standard configurable industrial control systems (Glattfelder and Schaufelberger, 2003).
In this paper these techniques shall be applied to an exponentially unstable plant controlled by a dynamic actuator with both stroke and slew saturations.
The control problem is defined in sect. 2, and a benchmark case is specified in sect. 3. In sect. 4 the effect of the actuator constraints on the radius of attraction is investigated for step inputs on both reference and load. It is shown that the standard awf structure is not able to enlarge the radius of attraction significantly here. Therefore a new approach is proposed and investigated in sect. 5 which is based on the override technique. It is shown by stability analysis and with simulations that the radius of attraction is substantially enlarged, up to the working range of the actuator.

## 2. THE CONTROL PROBLEM

Consider the control system given in Figure 1.

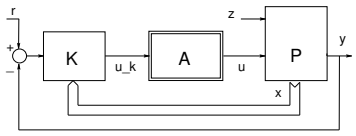


Figure 1. The control system with plant $P$, nonlinear actuator $A$, and controller $K$

*Plant P*
The manipulated variable $u$, the 'load' $z$ and the controlled variable $y$ shall be scalars.
The operating point of $P$ is determined by the steady state values of reference $\overline{r}$ and load $\overline{z}$, which require manipulated input values $\overline{u}$ for

equilibrium. Both $\overline{r}$ and $\overline{z}$ are specified on a bounded interval, such that the resulting $\overline{u}$ shall be within $u_{lo} < \overline{u} < u_{hi}$, that is within the design operating range of $A$.
$P$ is to be linear time invariant and in state space form, from where $y/u = G(s)$ is derived.
At least one pole of $G(s)$ shall be in the RHP (yielding the exponentially unstable open-loop modes), one or more is on the imaginary axis (for the stable modes), and one or more is in the LHP (for the asymptotically stable modes).
For simplicity let all state variables $\mathbf{x}$ be directly accessible. Thus no observer is needed for the state feedback part of $K$.

*Actuator A*
Here a typical electro-hydraulic actuator subsystem is considered, Fig. 2, (Glattfelder and Schaufelberger, 2003) p.218. The mechanical end stops of the servomotor piston are at $u_{lo}$, $u_{hi}$ (*stroke constraints*), and $v_{lo}$, $v_{hi}$ represent the flow constraints from the pilot servovalve (*slew constraints*), and $k_s$ is the gain of the P-controller. This model is embedded in the typical cascade structure, where the main controller outputs the position reference $u_c = r_s$.

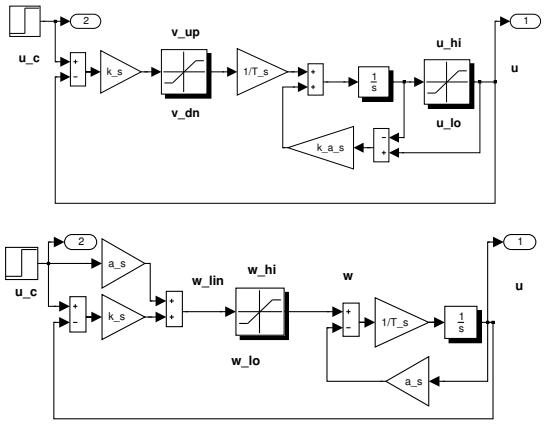


Figure 2. The actuator subsystem from physical modelling (top), approximation (bottom)

This model contains two nonlinear elements, which makes the stability analysis much more involved than for one nonlinear element. Therefore an approximate model is proposed here, Fig. 2 (bottom). It is similar to the one used in (Barbu *et al.*, 2002), but avoids the very high gain used there and has a single nonlinear element. – Let $a_s = 1.0$

$$\begin{aligned} &\text{Then} \quad w_{hi} = u_{hi}; && w_{lo} = u_{lo} \\ &\text{and} \quad \frac{d}{dt}u_{up} = \frac{1}{\tau_s}w_{hi}, && \frac{d}{dt}u_{dn} = \frac{1}{\tau_s}w_{lo} \end{aligned} \quad (1)$$

This determines $\tau_s$ and assumes symmetric saturation values. The approximate model is conservative with respect to the rate constraint, but reproduces the position constraint correctly, see Fig. 4.

*Controller K*
A standard state feedback is used with an output integral action and a static antiwindup feedback (gain $k_a$) acting on its input. $w$ is the output of the saturation element in Fig. 2, and $w_{lin}$ its input.

$$u_c = -\mathbf{k}^T\mathbf{x} + \frac{1}{s}\left[\frac{k_0}{\tau_0}(r-y) + k_a(w - w_{lin})\right] \quad (2)$$

The feedback gains can be determined by any linear design method. Here pole assignment to closed loop bandwidth $\Omega_1$ is used with $k_a := \Omega_1$, see (Glattfelder and Schaufelberger, 2003) p.282.

## 3. THE BENCHMARK

Let $P$ represent the inverted pendulum on a slider, around its upright position and valid for small inclination angles. The pendulum mass shall be concentrated at its center of gravity (cg). Denote the horizontal speed of its cg as $x_1$, the horizontal displacement between the cg's of pendulum and slider as $x_2$ and the horizontal speed of the slider as $x_3$. The actuator with state $x_4$ and input $w$ shall exert a horizontal force on the slider. The load $z$ is a horizontal force at the pendulum cg. Also the slider mass shall be much smaller than the pendulum mass. This finally yields as a suitable model:

$$\frac{x_1}{w} := \frac{1}{s\tau_4 + 1}\,\frac{1}{s^2\tau_3\tau_2 - 1}\,\frac{1}{s\tau_1}; \qquad \frac{x_1}{z} := \frac{1}{s\tau_1} \quad (3)$$

which shall be used in the sequel. Its poles are at $-1/\tau_4$ from the actuator; at $+1/\tau_2$ and $-1/\tau_3$ with $\tau_3 = \tau_2$ from the unstable inclination dynamics, and one at the origin. – Further

$$\tau_1 := 1.0;\ \tau_3 := \tau_2 := 0.20;\ \tau_4 := 0.20 \quad (4)$$

The *actuator saturations* are set to

$$u_{lo} = w_{lo} = -1.0; \quad u_{hi} = w_{hi} = +1.0 \quad (5)$$

The closed loop bandwidth is set to $\Omega_1 := 1.0/\tau_2$. Pole assignment to $(s + \Omega_1)^5 = 0$ yields

$$\begin{aligned} k4s &= 5(\Omega_1\tau_4) \\ k3s &= 10(\Omega_1\tau_3)(\Omega_1\tau_4) + (\tau_4/\tau_2) \\ k2s &= 10(\Omega_1\tau_2)(\Omega_1\tau_3)(\Omega_1\tau_4) + k4s \\ k1s &= 5(\Omega_1\tau_1)(\Omega_1\tau_2)(\Omega_1\tau_3)(\Omega_1\tau_4) \\ k0s &= (\Omega_1\tau_0)(\Omega_1\tau_1)(\Omega_1\tau_2)(\Omega_1\tau_3)(\Omega_1\tau_4) \end{aligned} \quad (6)$$

Then the state feedback is transformed to the cascade structure Fig. 3., with
- actuator loop $r_4 \to x_4$,
- inclination feedback $r_2 \to x_2$, using $x_3$,
- speed control $r_1 \to x_1$, with integral action $x_0$

$$\begin{aligned} &k4 = k4s - 1;\ \ k3 = k3s/k4s;\ k2 = k2s/k3s \\ &k1 = k1s/k2s;\ k0 = k0s/k1s; \end{aligned} \quad (7)$$

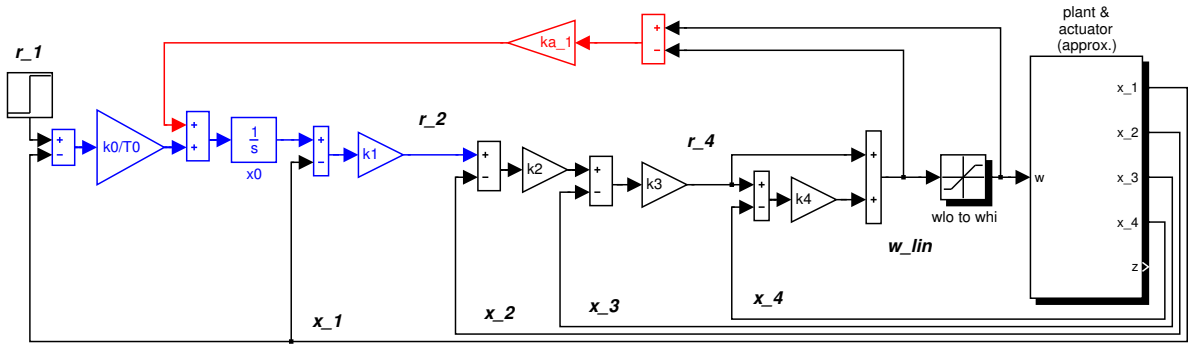


Figure 3. Structure of the awf control system

Finally for the awf gain

$$k_a = \Omega_1 \rightarrow ka_1 = ka/k1s \quad \text{or} \quad k_a = 0 \qquad (8)$$

Note that the actuator loop bandwidth results from the overall bandwidth design to $\Omega_1$.
For instance $\Omega_1 = 5$ yields $k_4 = 4.0$; see Fig.4.

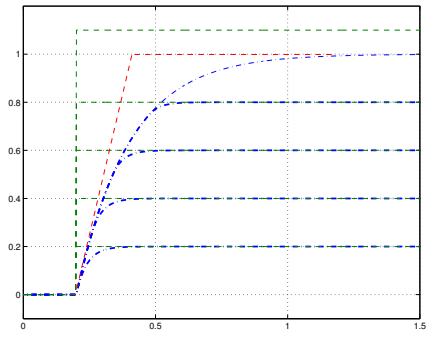

Figure 4. Step responses $r_4 \rightarrow x_4$ of the actuator loop with the approximate model

## 4. THE ANTIWINDUP APPROACH

### *4.1 Stability Analysis*

The plant $P$ and the controller $K$ in Fig. 1 are both not asymptotically stable. Thus the saturation element must be replaced by a parallel arrangement of a unity gain and a dead-span element with unity gain slopes and breakpoints at $w_{lo}$, $w_{hi}$. Then for the stability test (cf. (Glattfelder and Schaufelberger, 2003), p.284ff):

$$\Delta_{min} = \frac{w_{hi}}{w_{lin_{max}} - w_{hi}} \qquad (9)$$

and for the transfer function of the linear subsystem

$$F + 1 = \frac{1 + k_a \frac{1}{s}}{1 + R' \frac{1}{s} G} = \frac{d_G}{D_1}(s + k_a) \qquad (10)$$

where $d_G, D_1$ denote the characteristic polynomials of the plant and of the linear closed loop.

As will be shown next, the unstable root factor produces a strong phase shift of the Nyquist contour $F + 1$ into the LHP, which indicates a substantial reduction of the radius of attraction.
For the benchmark case:

$$F + 1 = \frac{(s + \frac{1}{\tau_4})\ (s^2 - \frac{1}{\tau_3 \tau_2})\ s^2}{(s + \Omega_1)^5} \ \frac{s + k_a}{s} \qquad (11)$$

where $(1/\tau_3) = (1/\tau_2) = (1/\tau_4) := \Omega_1$, and if the awf-gain is set to: $k_a := \Omega_1$, then finally

$$F + 1 = \frac{s}{s + \Omega_1} \ \frac{s - \Omega_1}{s + \Omega_1} \qquad (12)$$

Fig. 5 shows the corresponding Nyquist contour. The graphic stability test then requires the distance $-\Delta_{min} < -0.5$. Using the definition of $\Delta$ above, the maximum allowable deviations $w_{lin}$ are restricted to approximately three times the operating range $w_{hi}$.
For the case with no awf, set $k_a = 0.$:

$$F + 1 = \frac{s}{s + \Omega_1} \ \frac{s - \Omega_1}{s + \Omega_1} \ \frac{s}{s + \Omega_1} \qquad (13)$$

From the corresponding plot in Fig. 5 the shape of the Nyquist contour does not change significantly. Therefore the stability properties will not be significantly different.

In Fig. 5 the Nyquist contours are also drawn for the case where the unstable zero in $d_G$ is mirrored into the LHP, that is for the corresponding stable plant.

$$F + 1 = \frac{s}{s + \Omega_1} \quad \text{and} \quad \frac{s^2}{(s + \Omega_1)^2} \qquad (14)$$

Note the substantial difference in stability properties. The maximum allowable $w_{lin}$ tends to $\infty$ for the 'awf ON' case and to about 10 for 'awf OFF'.

Note that the effect of the actuator rate constraint $\tau_4$ on stability properties may be discussed as a generalization of this special case. However this shall not be pursued further here.

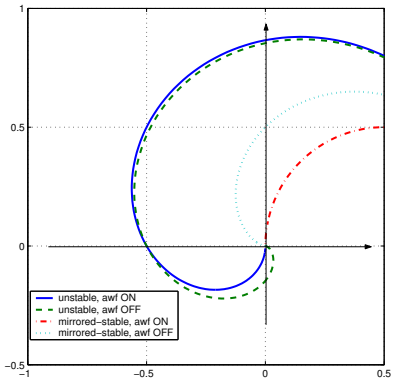


Figure 5. For the circle test: Nyquist contours for the antiwindup approach

### *4.2 Transient Responses*

Fig. 6 illustrates the responses of the system for the maximum stabilizable $r_1$ step.

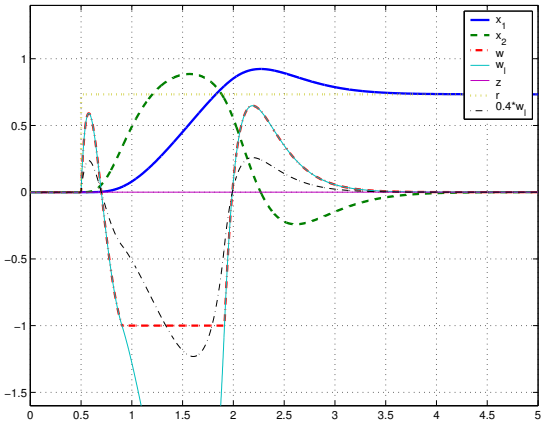


Figure 6. Response to the maximum stabilizable reference step

From simulations where reference steps were increased to the maximum stabilizable size $r_1$:

$$\begin{aligned} r_{1_{max}} &= 0.7190 \quad \text{for} \quad k_a = 0 \\ \text{and} \quad r_{1_{max}} &= 0.7335 \quad \text{for} \quad k_a = \Omega_1 \end{aligned} \tag{15}$$

This documents the weak influence of the awf gain on the radius of attraction.

Next the stability border from the simulation is correlated with the stability border from the graphic test Fig. 5, i.e. for $k_a := \Omega_1$. Using the off-axis circle test (or equivalently the Popov test), $\Delta_{min}$ is read from Fig.5:

$$\Delta_{StabT} = Re\{F(j\omega) + 1\} \text{ at } Im\{F(j\omega)\} = 0 \tag{16}$$

And from $w_{lin}(t)$ in the simulation Fig. 6, $w_{lin_{max}}$ is read as $1.22/0.40 = 3.05$ and this is converted to $\Delta_{Simul}$.

$$\Delta_{StabT} = 0.50 \quad \text{vs.} \quad \Delta_{Simul} = 0.49 \tag{17}$$

Thus the predictions from the stability test are nicely confirmed by the simulations.

Fig. 7 shows the response to the maximum admissible load step size for $k_a := \Omega_1$, from simulations:

$$z_{max} = 0.575 \tag{18}$$

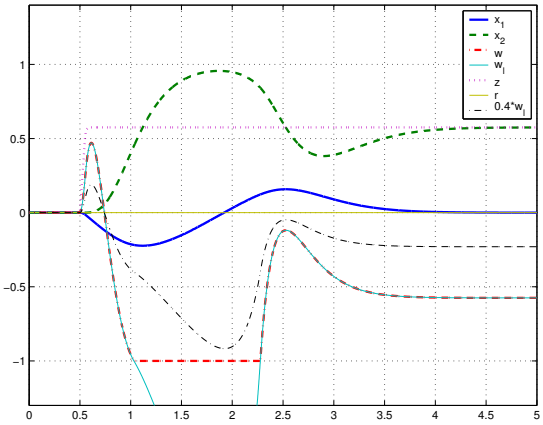


Figure 7. Response to the maximum stabilizable load step

*To summarize*, only a small part of the static working range of the actuator is utilizable. How this can be improved shall be shown next.

## 5. THE OVERRIDE APPROACH

### *5.1 The Basic Idea*

Consider again the control structure, Fig.3.
If $w_{lin}$ is driven beyond its saturation values, then the negative feedback through $k_3$, $k_2$ is inactivated, and thus the exponentially unstable inclination dynamics can no longer be stabilized. And this in turn is caused by excessive reference values $r_2(t)$ which are generated by the $r_1$-controller.
Therefore, in the override framework, $w_{lin}$ may be seen as a secondary output variable $y_c$, which has to be constrained to an operating range

$$\begin{aligned} & r_{c_{lo}} \le y_c \le r_{c_{hi}} \\ \text{with} \quad & r_{c_{lo}} = w_{lo} + \Delta_c; \quad \text{and} \quad r_{c_{hi}} = w_{hi} - \Delta_c \end{aligned} \tag{19}$$

where e.g. $\Delta_c := 0.05$ [1]
And the constraints on $y_c$ are implemented by overriding feedbacks on $w_{lin}$ through Min-Max-Selectors, Fig.8.
In contrast to the 'saturation and awf'-approach in sect. 4, now one of the inclination control loops is always closed and thus will see to stabilizing the exponentially unstable dynamics.

[1] This is a compromise between loosing actuation operating range and inadvertently having the stabilizing feedback inactivated by the saturations

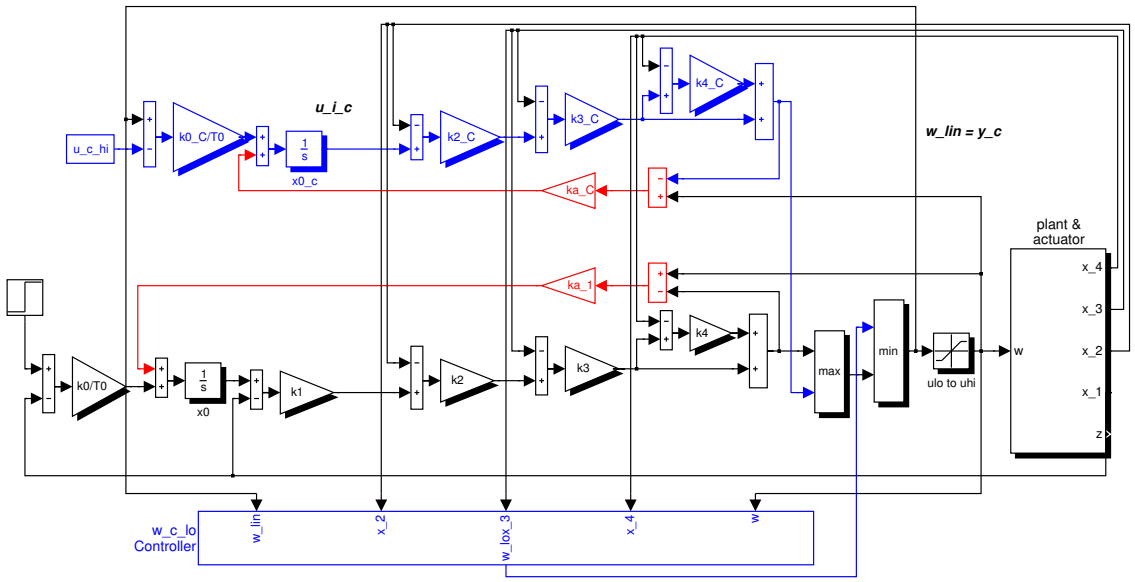


Figure 8. Structure of the override control system

In Fig. 8 these inclination feedbacks may be seen as 'slave' controllers in a cascade structure. The 'master' controller for the main variable $x_1$ is of PI(awf)-type, and for the override variable $y_c$ it is of I(awf)-type. The integral actions are inserted to suppress steady state offsets on $e_1$ and $e_c$. Then awf gains $ka_1, ka_C$ are needed to insure proper tracking. Two fully separate paths have been chosen here also for the 'slave' controllers (other structures are possible).

### *5.2 Designing the Override Loop*

The $x_1$-loop design is the same as in sect. 4.
For the override control loop the state feedback for the inclination stabilization is designed first and then the I(awf) feedback.
Denote the output of the integral action in the $y_c$ loop as $u_{i_C}$, see Fig. 8. Then

$$G_c = \frac{w_{lin}}{u_{i_C}} = \left[1 + \frac{1}{1+s\tau_4}k4c + \right.$$
$$\left. + \frac{(s\tau_2 k3c + k2c)}{(1+s\tau_4)(s\tau_3+1)(s\tau_2-1)}\right]^{-1}$$
$$= \frac{(1+s\tau_4)(s\tau_3+1)(s\tau_2-1)}{d_{3_C}} \quad \text{with}$$
$$d_{3_C} = s^3\tau_4\tau_3\tau_2 + s^2\tau_3\tau_2(k4c+1)$$
$$+ s\tau_2(k3c - (\tau_4/\tau_2) + (k2c - (k4c+1))$$

$$\rightarrow \quad G_c = -\,(1-s\tau_2)\,\frac{n_{3_C}}{d_{3_C}} \qquad (20)$$

where $d_{3_C}$ is the characteristic polynomial of the closed loops for actuator and inclination (which is asymptotically stable by design), and $n_{3_C}$ contains all zeros not in the RHP. Thus $G_c$ is an 'inverse-unstable' plant with a negative sign.
To implement the override action, the negative sign requires inverted signs on its I(awf)-controller, and 'crossing-over' the $u_{i_c}$'s upstream of the selectors, see (Glattfelder and Schaufelberger, 2003), p.377.
Furthermore general design rules recommend for the inverse-unstable plant dynamics an integrating output feedback, see Fig. 8,

$$u_{i_{C_{hi;lo}}} = -\,e_{c_{hi;lo}}\frac{k0\_C}{s\tau_0} = \frac{k0\_C}{s\tau_0}(y_c - u_{c_{hi;lo}}) \quad (21)$$

where $\tau_0 := \tau_2$, and also recommend to select the closed loop bandwidth at $\Omega_C \approx (1/\tau_2)$

Then from $(s+\Omega_C)^4 = 0$

$$k0c = (\Omega_C\tau_0)(\Omega_C\tau_2)(\Omega_C\tau_3)(\Omega_C\tau_4)$$
$$k4c = 4(\Omega_C\tau_4) + k0c(\tau_4/\tau_0)$$
$$k3c = 6(\Omega_C\tau_3)(\Omega_C\tau_4) + (\tau_4/\tau_2)k0c(\tau_3/\tau_0)$$
$$k2c = 4(\Omega_C\tau_2)(\Omega_C\tau_3)(\Omega_C\tau_4) - k0c(\tau_4/\tau_0) + k4c \quad (22)$$
$$\rightarrow \quad \text{(for the cascaded structure, Fig.8)}$$
$$k4\_C = k4c - 1; \quad k3\_C = k3c/k4c$$
$$k2\_C = k2c/k3c; \; k0\_C = k0c/k2c; ka\_C = \Omega_c/k2c \quad (23)$$

### *5.3 Nonlinear Stability Properties*

The nonlinearity in Fig. 8 has three inputs. This is equivalent to the one-input deadspan nonlinearity (Glattfelder and Schaufelberger, 2003), p. 114ff, producing the canonical structure required for the stability test. Then for the linear subsystem

$$F+1=\frac{1+\frac{ka_1}{s}}{1+R_1'\frac{1}{s}G_1}\cdot\frac{1+R_c'\frac{1}{s}G_c}{1+\frac{ka_C}{s}}= \tag{24}$$

$$\frac{d_{G_1}\cdot s}{(s+\Omega_1)^{N_1+1}}\,\frac{s+ka_1}{s}\,\frac{(s+\Omega_C)^{N_C+1}}{d_{G_C}\cdot s}\,\frac{s}{s+ka_C} \tag{25}$$

where from the basic idea of sect. 5.1, the characteristic open loop polynomial $d_{G_C}$ of degree $N_C$ contains the exponentially unstable poles of the plant, and $d_{G_1}$ of degree $N_1$ stands for the series connection of $d_{G_C}$ with additional but stable dynamics $d_{G_1^+}$ of degree $N_1-N_C$.
Thus by construction of the override system, the exponentially unstable poles (zeros of $d_{G_C}$) always cancel in $F+1$, that is

$$F+1=d_{G_1^+}\,\frac{(s+\Omega_C)^{N_C+1}}{(s+\Omega_1)^{N_1+1}}\cdot\frac{s+ka_1}{s+ka_C} \tag{26}$$

For the benchmark example $N_1=4;\ N_C=3$
and for compensating awf: $ka_i=\Omega_i;\ i=1,C$

$$d_{G_1^+}=s;\qquad d_{G_C}=(s+\frac{1}{\tau_4})(s^2-\frac{1}{\tau_3\tau_2})$$

$$F+1\to\frac{s}{(s+\Omega_1)}\,\frac{(s+\Omega_C)^3}{(s+\Omega_1)^3} \tag{27}$$

and as typically $\Omega_C:\approx\Omega_1$, the Nyquist contour of $F+1$ will now avoid the LHP.
Fig. 9 illustrates this for $\Omega_C\tau_2=[1.3,\ 1.2,\ 1.1]$

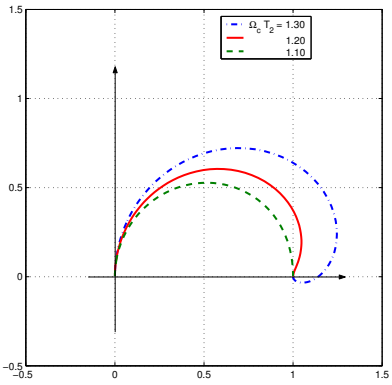


Figure 9. Nyquist contours for the override system

This indicates a very large radius of attraction, allowing large inputs $w_{lin_{max}}$ and thus either large reference steps $r_1$ or, for step loads, resulting steady state offsets $\overline{w}$ close to the operating constraint setpoints on $w_{lin}$. Fig. 10 confirms this by the response to a large reference step $r_1=2.0$ (top) and to a load step $z_1$ to 0.90 (bottom), with $\Omega_cT_2=1.20$, and with constraint setpoints at $w_{hi}=0.970;\ w_{lo}=-0.970$.

*To summarize*, the region of attraction for reference steps has been extended from 0.7335 to near-infinity, and for load steps from 0.575 up to 0.90, i.e. close to the actuator working range.

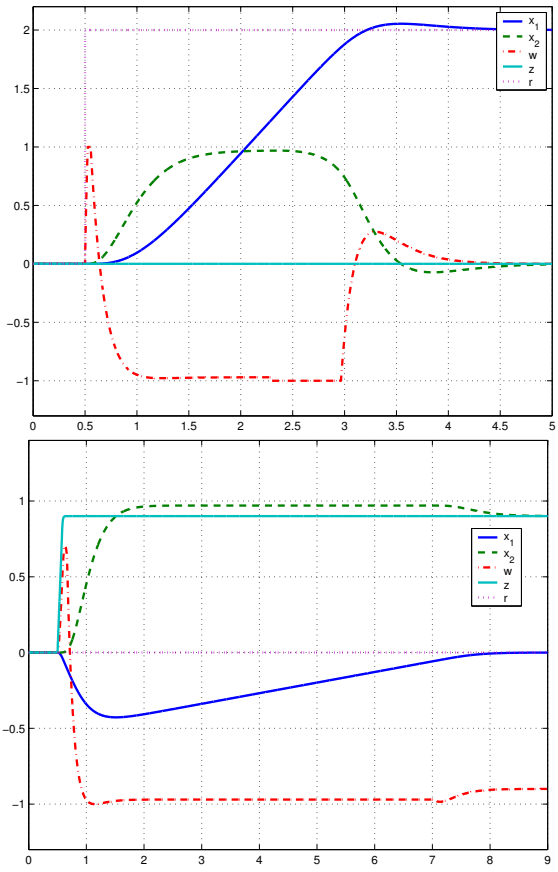


Figure 10. Step responses for the override system

## 6. SUMMARY

The novel application of the override concept on an exponentially unstable system has enlarged its radius of attraction up to what practical applications would require.

## REFERENCES


Barbu, C., R. Reginatto, A.R. Teel and L. Zaccharian (2002). Anti-windup for exponentially unstable linear systems with rate and magnitude input limits. In: *Actuator Saturation Control* (V. Kapila and K.M. Grigoriadis, Eds.). pp. 1–31. Marcel Dekker Inc., ISBN 0-8247-0751-6.

Glattfelder, A.H. and W. Schaufelberger (2003). *Control Systems with Input and Output Constraints*. Springer Verlag Limited, ISBN 1-85233-387-1. London.

Khalil, H.K. (2002). *Nonlinear Systems*. 3nd ed.. Prentice Hall, ISBN 0-13-067389-7.

Tarbouriech, S. and G. Garcia (2002). Output feedback compensators for linear systems with position and rate bounded actuators. In: *Actuator Saturation Control* (V. Kapila and K.M. Grigoriadis, Eds.). pp. 247–272. Marcel Dekker Inc., ISBN 0-8247-0751-6.